In-beam γ-ray spectroscopy of ^{136}Te at relativistic energies

V. Vaquero,[1] A. Jungclaus,[1,*] P. Doornenbal,[2] K. Wimmer,[3,2] A. M. Moro,[4] K. Ogata,[5] T. Furumoto,[6] S. Chen,[2,7] E. Nácher,[1]
E. Sahin,[8] Y. Shiga,[9] D. Steppenbeck,[2] R. Taniuchi,[2,3] Z. Y. Xu,[10] T. Ando,[3] H. Baba,[2] F. L. Bello Garrote,[8] S. Franchoo,[11]
K. Hadynska-Klek,[8] A. Kusoglu,[12,13] J. Liu,[10] T. Lokotko,[10] S. Momiyama,[3] T. Motobayashi,[2] S. Nagamine,[3] N. Nakatsuka,[14]
M. Niikura,[3] R. Orlandi,[15] T. Y. Saito,[3] H. Sakurai,[2,3] P. A. Söderström,[2] G. M. Tveten,[8] Zs. Vajta,[16] and M. Yalcinkaya[12]

[1]*Instituto de Estructura de la Materia, CSIC, E-28006 Madrid, Spain*
[2]*RIKEN Nishina Center, 2-1 Hirosawa, Wako, Saitama 351-0198, Japan*
[3]*Department of Physics, University of Tokyo, 7-3-1 Hongo, Bunkyo, Tokyo 113-0033, Japan*
[4]*Departamento de FAMN, Universidad de Sevilla, Apartado 1065, E-41080 Sevilla, Spain*
[5]*Research Center for Nuclear Physics, Osaka University, Ibaraki 567-0047, Japan*
[6]*Graduate School of Education, Yokohama National University, Yokohama 240-8501, Japan*
[7]*School of Physics and State Key Laboratory of Nuclear Physics and Technology, Peking University,
Bejing 100871, People's Republic of China*
[8]*Department of Physics, University of Oslo, NO-0316 Oslo, Norway*
[9]*Department of Physics, Rikkyo University, 3-34-1 Nishi-Ikebukuro, Toshima, Tokyo 172-8501, Japan*
[10]*Department of Physics, The University of Hong Kong, Pokfulam, Hong Kong*
[11]*Institut de Physique Nucléaire Orsay, IN2P3-CNRS, F-91406 Orsay Cedex, France*
[12]*Department of Physics, Faculty of Science, Istanbul University, Vezneciler/Fatih, TR-34134 Istanbul, Turkey*
[13]*ELI-NP, Horia Hulubei National Institute of Physics and Nuclear Engineering, RO-077125 Magurele, Romania*
[14]*Department of Physics, Faculty of Science, Kyoto University, Kyoto 606-8502, Japan*
[15]*Advanced Science Research Center, Japan Atomic Energy Agency, Tokai, Ibaraki 319-1195, Japan*
[16]*MTA Atomki, P.O. Box 51, Debrecen H-4001, Hungary*

The reduced transition probability B($E2$; $0_1^+ \rightarrow 2_1^+$) to the first excited 2^+ state of the neutron-rich nucleus ^{136}Te, with two protons and two neutrons outside the doubly magic ^{132}Sn core, was measured via Coulomb excitation at relativistic energies at the RIKEN Radioactive Isotope Beam Factory. A value of B($E2$) = 0.191(26) e^2b^2 was extracted from the measured inelastic scattering cross section on an Au target taking into account the contributions from both Coulomb and nuclear excitations. In addition, an upper limit for the transition strength to a 2^+ state of mixed-symmetry character in the excitation energy range of 1.5–2.2 MeV was determined and compared to the predictions of various theoretical calculations. Because of the high statistics gathered in the present experiment the error of the deduced B($E2$) value is dominated by the systematic uncertainties involved in the analysis of Coulomb excitation experiments at beam energies around 150 MeV/u. Therefore, the latter are for the first time assessed in detail in the present work.

I. INTRODUCTION

Since the pioneering study of the neutron-rich Te isotopes by Radford and collaborators [1] using low-energy Coulomb excitation of radioactive beams in inverse kinematics at the Holifield Radioactive Ion Beam Facility (HRIBF) of the Oak Ridge National Laboratory (ORNL) more than 15 years ago, significant theoretical effort was devoted trying to achieve a better understanding of these nuclei close to the doubly magic ^{132}Sn. In particular the low value of the reduced transition probability to the first excited 2^+ state of ^{136}Te at an excitation energy of $E_x = 607$ keV, B($E2$; $0_1^+ \rightarrow 2_1^+$) = 0.103(15) e^2b^2 [in the following abbreviated B($E2$)], which implied

a significant asymmetry of this quantity with respect to the $N = 82$ shell closure in the chain of Te isotopes [for ^{132}Te a value of B($E2$) = 0.172(17) e^2b^2 was measured in the same work], was considered as a real surprise at that time. Later this low B($E2$) value was confirmed by the preliminary results of a fast timing experiment performed at ISOLDE which yielded B($E2$) = 0.122(24) e^2b^2 [2]. In 2011 it was reported that the data analysis, which led to the results presented in Ref. [1], was based on an erroneous assumption on the target thickness [3]. Consequently, corrected B($E2$) values were quoted for ^{132,134,136}Te which, although slightly larger as compared to Ref. [1] [B($E2$) = 0.216(22) e^2b^2 for ^{132}Te and B($E2$) = 0.122(18) e^2b^2 for ^{136}Te], still reflected the asymmetry mentioned above. While shell model calculations were not able to reproduce this peculiar behavior of the $E2$ strength [4], the calculations performed by Terasaki *et al.*

using the quasiparticle random phase approximation (QRPA) traced it to a reduced neutron pairing above the $N = 82$ gap which causes a neutron dominance in the wave function of the 2_1^+ state of ^{136}Te [5].

Very recently a new measurement was reported upon [6], performed again at the HRIBF using Coulomb excitation in inverse kinematics. This time, however, a heavier titanium target was used as compared to the carbon target which had been employed in the first experiment. The new value of B($E2$) = 0.181(15) e^2b^2 is in clear conflict with the previously reported results.

In view of this inconsistent body of experimental information a re-measurement of the B($E2$; $0_1^+ \rightarrow 2_1^+$) value in ^{136}Te using an independent approach seemed highly desirable. We therefore conducted an experiment at the Radioactive Isotope Beam Factory (RIBF), operated by the RIKEN Nishina Center and the Center for Nuclear Study of the University of Tokyo, using the technique of Coulomb excitation at relativistic energies. An additional motivation for this measurement was the search for an excited 2^+ state of mixed proton-neutron symmetry in ^{136}Te, which several theoretical studies predict to exist in the excitation energy range of 1.5–2.2 MeV [4,7–9]. The study of the decay properties of such a 2_{ms}^+ state, the isovector analog of the 2_1^+ level, in ^{136}Te, in comparison to those of the recently observed 2_{ms}^+ state in ^{132}Te [3], constitutes an alternative approach to probe the proton-neutron balance of the nuclear wave function. Note that at relativistic energies the Coulomb excitation cross section for a 2^+ state is nearly independent on the excitation energy. Therefore, the population of higher-lying excited 2^+ states in this experiment is favorable as compared to the studies using low-energy Coulomb excitation, in which the cross section for the excitation of a 2^+ level decreases with its excitation energy.

Finally, the high statistics gathered in the present experiment allowed one for the first time to evaluate in detail the validity of the chosen analysis approach. The latter will be described in detail in this article to serve as a guideline for the evaluation of the different systematic uncertainties involved in the analysis of other experiments using the same technique but accumulating less statistics.

II. EXPERIMENT

The experiment was carried out at the RIBF at RIKEN. A primary beam of ^{238}U at 345 MeV/u bombarded a 4-mm-thick beryllium target located at the entrance of the BigRIPS fragment separator [10]. The fission products around ^{136}Te were selected and purified by employing the Bρ-ΔE-Bρ method through a combination of magnetic rigidity (Bρ) selection and two wedge-shaped aluminium degraders. The particle identification was performed on an event-by-event basis using the ΔE-Bρ-TOF method, where the energy loss ΔE was measured by an ionization chamber located at the focal plane F7, Bρ was determined from position measurements using parallel plate avalanche counters (PPACs), and the time of flight (TOF) was measured with two plastic scintillators located at the focal points F3 and F7. The atomic number (Z) and the mass-over-charge (A/Q) ratio of each ion were determined with this method [11]. The primary beam intensity
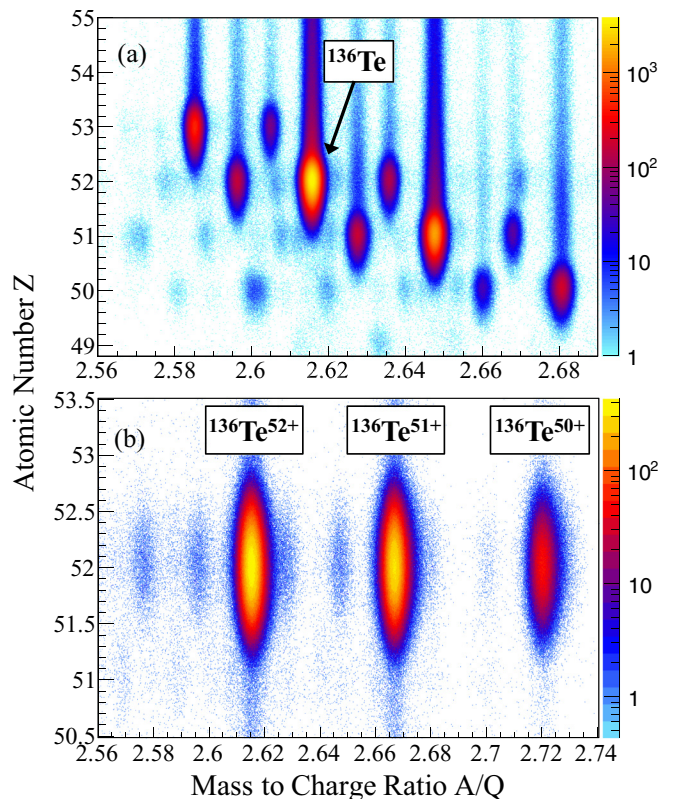

FIG. 1. Particle identification plots for (a) BigRIPS and (b) the ZeroDegree spectrometer requiring the identification of ^{136}Te ions in BigRIPS obtained with the Au target. Note that the ^{136}Te ions were observed in different charge states in ZeroDegree.

was kept below 2.5 pnA to limit the counting rates in the beam detectors, in particular the ionization chambers, to such a level that a clean particle identification can be achieved. The particle identification plot obtained in this way is shown in Fig. 1(a).

After the selection and identification, the secondary beams were transported to the focal point F8 where they impinged in two different runs on reaction targets consisting of 950 mg/cm^2 Au and 535 mg/cm^2 C, respectively. In total 2.36×10^8 ^{136}Te ions interacted with the Au target while 6.72×10^7 impinged on the C target. The high-Z Au target ($Z = 79$) was used to induce Coulomb excitation, while the low-Z C target ($Z = 6$) allowed one to extract the nuclear contribution to the inelastic scattering cross section measured with the Au target. At the center of the target, the energies of the ^{136}Te ions were 139 MeV/u (corresponding to $\beta = 0.493$) and 140 MeV/u ($\beta = 0.494$) for the Au and C targets, respectively [165 (110) and 165 (112) MeV/u before (after) the target]. The scattering angles of the elastically and inelastically scattered ions were measured with two PPACs installed upstream and one PPAC installed downstream of the reaction target. The reaction products were identified by the ZeroDegree spectrometer [10] using again the previously described ΔE-Bρ-TOF method. Figure 1(b) shows the ZeroDegree particle identification following the interaction of ^{136}Te ions with the Au target. Note that the ^{136}Te ions were

detected in the ZeroDegree spectrometer in three different charge states, namely 50% fully stripped, 42% hydrogenlike, and 8% heliumlike (the corresponding numbers for the C target are 64%, 33%, and 3%, respectively).

To measure γ rays emitted following the decay of excited states of the reaction products, the target was surrounded by the DALI2 spectrometer [12], a high-efficiency γ-ray detector array consisting of 186 NaI(Tl) detectors covering angles from 20° to 150°. To reduce the low-energy bremsstrahlung background, the beam pipe at the F8 focus was enclosed by 1-mm lead and 1-mm tin shields. A DALI2 energy calibration was performed using ^{60}Co, ^{88}Y, and ^{137}Cs sources. The full-energy-peak efficiency and energy resolution (FWHM) were obtained to be around 15% and 6%, respectively, at 1.33 MeV (^{60}Co). This efficiency value is in good agreement with simulations performed using the GEANT4 code [13]. To reduce the dead time of the data acquisition system, during the present experiment only the 92 NaI(Tl) crystals placed at forward angles $\theta < 60°$ in the laboratory frame (layers 10 and 11 plus the forward wall [12]) were used. In this angular range, because of the Lorentz boost and the background properties, the peak-to-background ratio was largest. Considering only this subarray and assuming prompt emission, the efficiency reduced from 24% to 13% for a γ ray with an energy of 600 keV emitted by ions moving with a velocity of $\beta = 0.5$. To increase the detection efficiency for high-energy γ rays and to improve the peak-to-total ratio over the full energy range an add-back algorithm was applied for the data taken with the C target. All energy depositions registered in NaI crystals within a range of 15 cm from the center of the crystal with the highest energy signal were summed. Doppler correction was then performed assuming that the largest energy deposition corresponds to the first interaction of the γ ray in the array and using the midtarget velocity. Add-back was applied to increase the statistics of the γ-ray spectra and in particular for the analysis of $\gamma\gamma$ coincidences. However, all cross sections reported in the present work were determined from γ-ray spectra without add-back. The reason for that is that the γ-ray efficiency applying the add-back algorithm strongly depends on the background which is not included in the GEANT4 simulations.

III. RESULTS

A. γ-ray spectra and level scheme

The Doppler-shift corrected γ-ray spectrum from inelastic scattering of ^{136}Te on the C target is shown in Fig. 2(a). Five lines at energies around 330, 400, 600, 810, and 960 keV are visible in this spectrum. From spontaneous fission and β-decay studies [14–16], γ rays with 353, 423, and 607 keV are known to form the $6_1^+ \rightarrow 4_1^+ \rightarrow 2_1^+ \rightarrow 0_1^+$ sequence in ^{136}Te and we therefore identify the first three lines in the spectrum of Fig. 2(a) with these transitions. Furthermore, a 962-keV γ ray was observed in Ref. [15] and assigned as decaying from a (2_2^+) state at 1568 keV to the 2_1^+ level at 607 keV. Most probably this transition corresponds to the highest-energy line observed in Fig. 2(a). In addition, a γ ray with an energy of 810(15) keV is observed for
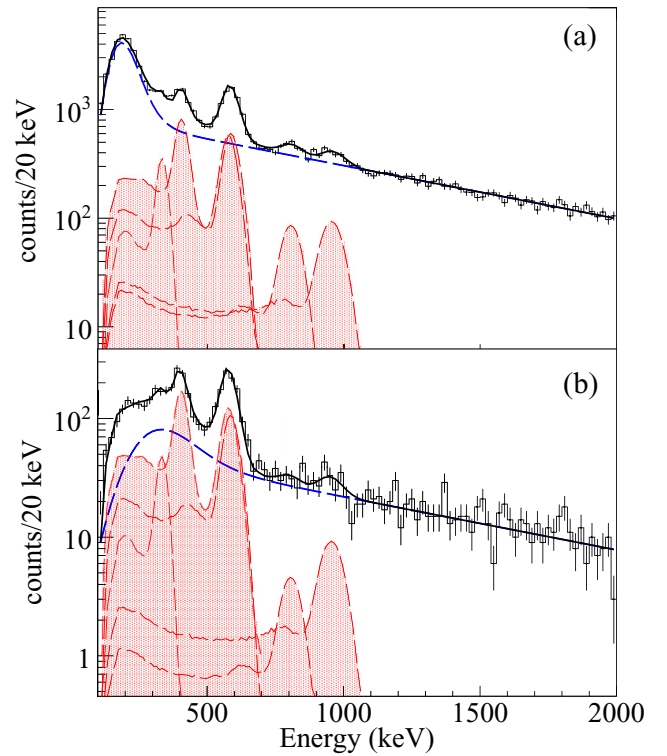
FIG. 2. (a) Doppler-shift corrected γ-ray spectrum from inelastic scattering of ^{136}Te on the C target. The fit to the experimental spectrum is shown as a thick black line which is the sum of the background (blue dashed line) and the simulated DALI2 response for γ rays with energies of 353, 423, 607, 810, and 962 keV (red dashed lines). No cut on the γ-ray multiplicity was applied. (b) Same as (a), but for the one-neutron transfer reaction C(^{137}Te, ^{136}Te). Here, only events with multiplicity $M_\gamma < 4$ are considered. In both parts of the figure add-back was applied.

the first time in the present experiment. The background in the spectrum shown in Fig. 2(a) can be parametrized by the sum of two exponential functions cut off at low energy with an error function. The experimental spectrum is then nicely reproduced by the sum of this background and the simulated response function of the DALI2 array for γ rays with energies of 353, 423, 607, 810, and 962 keV. Note that the feeding of the 2_1^+ level from the 4_1^+ state is simulated as a cascade because the finite lifetime of the 4_1^+ state (see below) affects the position of the line corresponding to the $2_1^+ \rightarrow 0_1^+$ transition. As shown in Fig. 2(b), the same five γ transitions are also observed following the population of ^{136}Te via the one-neutron knockout reaction from ^{137}Te, although with different relative intensities. A comparison between the two spectra shown in Fig. 2 nicely illustrates the very different shape of the background, in particular at low energy, in these two reaction channels leading to the same final nucleus.

To obtain information about the placement of the new 810-keV transition in the level scheme of ^{136}Te, $\gamma\gamma$-coincidence spectra were produced using the data from inelastic scattering with a gate on either the 607-keV, $2_1^+ \rightarrow 0_1^+$ transition or the 962-keV, $(2_2^+) \rightarrow 2_1^+$ transition; see Fig. 3. Because the moderate energy resolution of DALI2 does not allow one to
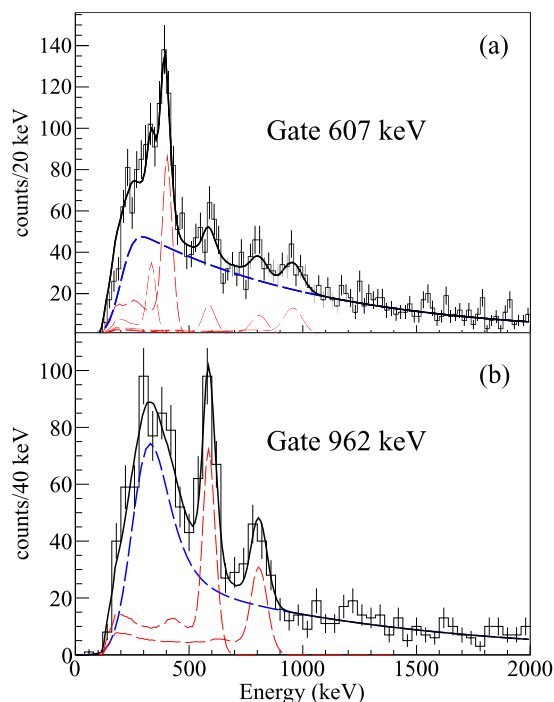
FIG. 3. $\gamma\gamma$-coincidence spectra for ^{136}Te on the C target with gate on (a) the 607-keV, $2^+_1 \rightarrow 0^+_1$ transition and (b) the 962-keV, $(2^+_2) \rightarrow 2^+_1$ transition. In both parts of the figure add-back was applied and only events with multiplicity $M_\gamma < 6$ were considered.

FIG. 4. Level scheme of ^{136}Te including the new transition with an energy of 810(15) keV (see text for details). All energies are quoted in keV. The feeding (normalized to that of the first excited 2^+ state) of all excited states of ^{136}Te populated in the present experiment via the inelastic scattering (one-neutron knockout) reaction on a C target is quoted above (below) each level.

perform a clean background subtraction, in addition to the lines corresponding to the 353-, 423-, 810-, and 962-keV transitions, also one at 607 keV is observed in the spectrum shown in Fig. 3(a). This self-coincidence has its origin in the contributions from the Compton background of the higher-energy transitions to the energy gate on the 607-keV line (compare Fig. 2). The gate on the 962-keV transition, in contrast, is expected to be much cleaner because of the lower background at higher energies and the fact that no γ rays are observed above 1 MeV. The coincidence spectrum in Fig. 3(b) shows that in addition to the 607-keV ground-state transition also the new 810-keV transition is observed in coincidence with the 962-keV line suggesting its placement on top of the (2^+_2) state as shown in Fig. 4. Included in Fig. 4 is also the relative feeding of the excited states of ^{136}Te populated via either inelastic scattering or one-neutron knockout. Note that the 4^+_1 and 6^+_1 yrast states are stronger populated relative to the 2^+_1 state in the one-neutron knockout reaction while the population of the yrare (2^+_2) level is comparable in the two reactions.

The Doppler-corrected γ-ray spectrum measured in co-incidence with ^{136}Te ions detected in both BigRIPS and the ZeroDegree spectrometer for the Au target is shown in Fig. 5(a). Only a single line corresponding to the decay of the first excited 2^+ state at 607 keV is observed in the energy range up to 2 MeV. Because for the relativistic beam energies used in the present experiment the probability for multistep Coulomb excitation is very small, the nonobservation of the transitions emitted in the decay of the 4^+_1 and 6^+_1 states is
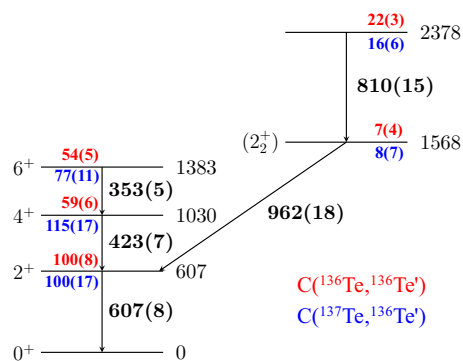
expected. However, a second 2^+ state could have been excited and its decay observed in the present experiment if the B($E2$) transition probability would have been sufficiently large.

As mentioned in the introduction several theoretical calculations predict the existence of an excited 2^+ state with mixed proton-neutron symmetry in ^{136}Te in the excitation energy range 1.5–2.2 MeV. Such a mixed-symmetry 2^+_{ms} state is expected to decay via a strong $M1$ transition to the 2^+_1 and a weak $E2$ to the 0^+_1 level. As illustrated by the difference between the experimental spectrum and the fitted DALI2 response shown in Fig. 5(b), in addition to the 607-keV ground-state transition no additional γ ray is observed in the energy range up to 2 MeV in the present experiment following the excitation of the ^{136}Te beam on the Au target. In particular, we note that the 962-keV $(2^+_2) \rightarrow 2^+_1$ transition, which was observed with the C target (see Fig. 2), is absent in the spectrum shown in Fig. 5(a). To optimize the resolution for the 607-keV line in this spectrum Doppler correction was performed using $\beta = 0.448$ corresponding to the velocity of the ^{136}Te ions behind the target. However, the search for additional lines in the spectrum was performed for a wide range of β values. Based on Monte Carlo simulations and the difference spectrum shown in Fig. 5(b) observational lower limits of 10% and 14% relative to the intensity of the 607-keV line have been determined for hypothetical γ-ray energies of 0.9 MeV and 1.6 MeV, respectively. The estimation of B($E2$; $0^+_1 \rightarrow 2^+_{ms}$) limits from these values will be discussed in Sec. VII.

Finally, we note in passing that in the present experiment, in addition to the 607-keV $2^+_1 \rightarrow 0^+_1$ transition, two γ rays with energies of 3.6(1) and 4.2(1) MeV, respectively, have been observed for the first time. They depopulate a state at an excitation energy of 4.2(1) MeV and the 3.6(1) MeV γ ray corresponds to a decay branch to the 2^+_1 state. This new excited state will be discussed in detail in a forthcoming publication. It is sufficient to mention here that this indirect feeding of the 2^+_1 level will correctly be taken into account in the determination of the B($E2$; $0^+_1 \rightarrow 2^+_1$) value presented in Sec. VI.
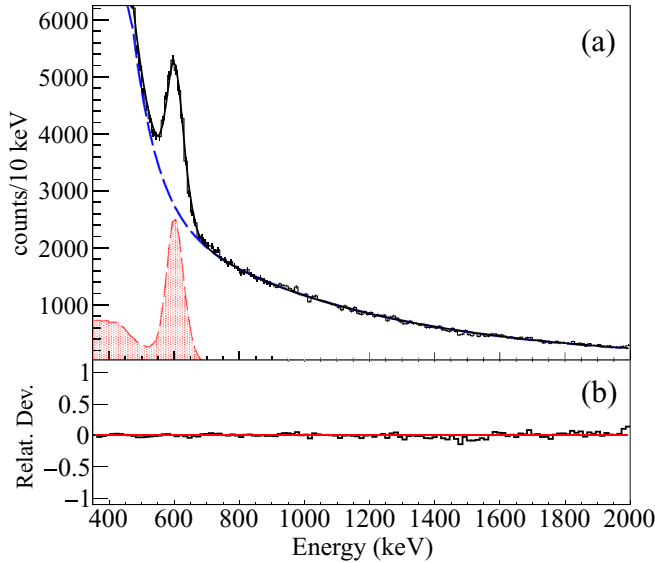
FIG. 5. (a) Doppler-shift corrected γ-ray spectrum from inelastic scattering of ^{136}Te on the Au target. The fit to the experimental spectrum is shown by the thick black line, which is composed of a two-exponential function describing the background (blue dashed line) and the simulated response function of DALI2 for the 607-keV $2_1^+ \rightarrow 0_1^+$ transition (red dashed line). No cut on the γ-ray multiplicity and no add-back was applied. (b) Relative difference between the experimental and simulated spectra shown in (a).

B. Direct lifetime determination based on the observed Doppler shifts

Both the 2_1^+ and 4_1^+ states in ^{136}Te are known to have lifetimes of tens of picoseconds [6]. This implies that the 607- and 423-keV γ rays are emitted mainly after the ions already left the target. If Doppler correction is performed using the midtarget velocity and assuming emission from the center of the target, these lines are shifted to smaller energies as compared to the nominal values (all detectors are placed at $\theta < 60°$). Therefore, as already was demonstrated in Ref. [17], estimates of the excited-state lifetimes can be obtained from a comparison between the experimental line shapes and Monte Carlo simulations.

In Fig. 6(a) the experimental line shape of the 607-keV line measured with DALI2 for the Au target is compared to GEANT4 simulations assuming a prompt decay of the 2_1^+ state. Clearly the experimental line shape is not reproduced by these simulations. Only when a finite lifetime around $\tau(2_1^+) = 33$ ps is assumed, a good agreement is obtained [see Fig. 6(b)]. In the spectrum taken with the C target in addition to the 607-keV line also the 423-keV transition emitted in the decay of the 4_1^+ state is observed [compare Fig. 2(a)]. Keeping the lifetime of the 2_1^+ state fixed, $\tau(2_1^+) = 33$ ps, and considering both a direct population of the 2_1^+ state as well as a cascade of two γ rays emitted following the population of the 4_1^+ level a longer lifetime around 98 ps is needed for the 4_1^+ state to describe the experimental spectrum [compare Figs. 6(c) and 6(d)]. This value has to be considered as effective lifetime of the 4_1^+ state because the relative intensities quoted in Fig. 4 indicate significant feeding from the 6_1^+ state. Unfortunately,
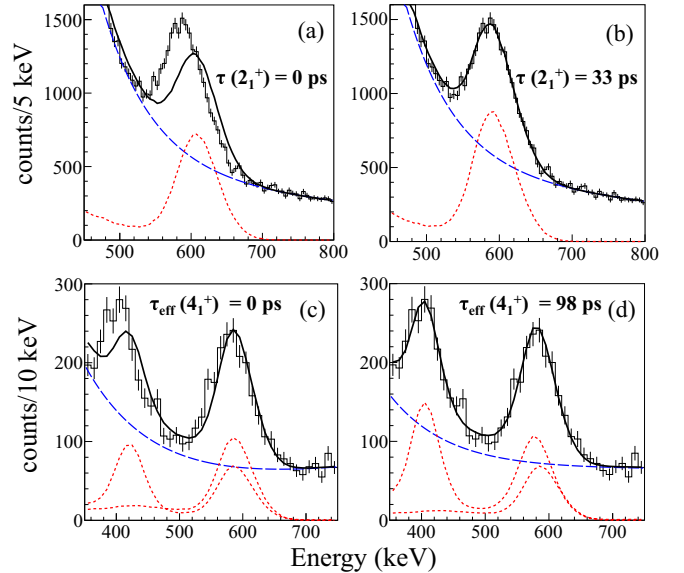

FIG. 6. (a) Comparison between the experimental shape of the 607-keV line for the Au target (black histogram) and GEANT4 simulations (black line) assuming $\tau(2_1^+) = 0$ ps; (b) same as (a) but assuming $\tau(2_1^+) = 33$ ps; (c) comparison between the experimental shapes of the 423- and 607-keV lines (black histogram) for the C target and GEANT4 simulations (black line) assuming $\tau(2_1^+) = 33$ ps and $\tau_{\mathrm{eff}}(4_1^+) = 0$ ps, (d) same as (c) but assuming $\tau_{\mathrm{eff}}(4_1^+) = 98$ ps. In parts (a) and (b) no add-back was applied and the γ-ray multiplicity was limited to $M_\gamma = 1$ while in parts (c) and (d) add-back was applied and only events with $M_\gamma = 2$ were considered. In all cases Doppler correction performed using the midtarget velocity.

because of the increasing background in the low-energy region of the spectrum and the vicinity to the 423-keV line, it was not possible to deduce any information with respect to the unknown lifetime of the 6_1^+ state from an analysis of the line corresponding to the 353-keV transition. Final values of $\tau(2_1^+) = 33(15)$ ps and $\tau_{\mathrm{eff}}(4_1^+) = 98(50)$ ps were deduced from the experimental spectra shown in Fig. 6. From the fit of the simulated DALI2 response functions assuming vanishing excited state lifetimes to the two lines observed around 810 and 962 keV in Fig. 2(a), γ-ray energies of 810(15) and 962(18) keV have been deduced. The agreement of the latter value with the literature value of 961.72(5) keV [15] suggests that the lifetime of the (2_2^+) level at 1568 keV is short.

Note that while the accuracy which can be achieved using this technique is obviously very limited when unsegmented scintillator arrays such as DALI2 are used for γ-ray detection as in the present experiment, it becomes a precision tool when position-sensitive Ge detectors are employed for in-beam spectroscopy at relativistic energies [18,19] and will show its full power with γ-ray tracking arrays such as AGATA [20] and GRETA [21] in the future.

IV. DETERMINATION OF EXCLUSIVE SCATTERING CROSS SECTIONS

To determine experimental differential inelastic scattering cross sections, the γ-ray yield has to be measured as a
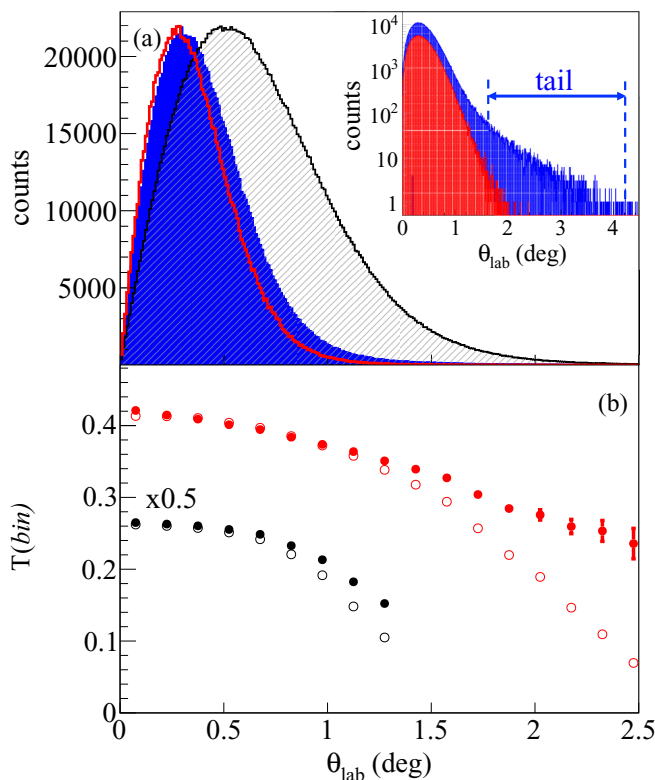
FIG. 7. (a) Angular distributions of the ions which have been identified as ^{136}Te in BigRIPS without target (red line) and for the C (blue area) and Au (gray area) targets, respectively. Note that the three curves have been scaled to the same height for better comparability. The inset shows the angular distribution of the ^{136}Te ions for the C target [filled blue curve, same as blue curve in (a)] on a logarithmic scale in comparison to the one obtained when in addition the detection of a fully stripped ^{136}Te ion in the ZeroDegree spectrometer is required (filled red curve). (b) Transmission curves for those ^{136}Te ions which are detected in the ZeroDegree spectrometer in the fully stripped charge state for the C (black, multiplied by 0.5) and Au (red) targets, respectively, before (open circles) and after correction for reaction losses (bullets). Angular bins of $\Delta\theta_{lab} = 0.15°$ were used. See text for details.

function of the scattering angle. In the present experiment the latter is measured using the information from the three PPACs installed in front of and behind the target position. The proper alignment of all beam detectors used in the reconstruction of the incoming and outgoing beam trajectories was checked by confirming a flat distribution of the azimuthal scattering angle. In Fig. 7(a) the angular distributions of the ^{136}Te ions identified in BigRIPS are shown for the runs without target (empty frame) and with the C and Au targets inserted at target position. Note that in the following the expression cross-section angular distribution always refers to $d\sigma/d\theta_{lab}$ [which includes the $\sin(\theta)$ and corresponds to what is really measured], in contrast to the differential cross section $d\sigma/d\Omega$. All three distributions can be fitted with Gaussian curves multiplied by $\sin(\theta)$ yielding width parameters σ of 4.8 mrad, 5.4 mrad, and 8.8 mrad, respectively. The angular resolution measured without target reflects the uncertainty of the position measure-

ments in the PPAC detectors. The measured value $\sigma = 4.8$ mrad can be reproduced in Monte Carlo simulations assuming a position resolution of $\sigma_x = \sigma_y = 0.73$ mm for all PPAC detectors involved in the measurement of the scattering angle. With the C and Au targets in the beam an additional contribution stemming from the angular straggling, mainly from multiple elastic scattering in the target material, leads to considerably worse angular resolutions. This angular straggling was estimated with the code ATIMA [22] based on the energy before the target and the target thickness to 2.3/8.0 mrad for the C/Au targets. Combining the contributions from the position measurement and the straggling, values of 5.3/9.3 mrad are obtained in somewhat good agreement with the experimental observation.

In the next step, separate γ-ray spectra were produced for different ranges of the scattering angle. To determine the cross-section angular distribution for the excitation of the 2_1^+ state, angular bins of $\Delta\theta_{lab} = 0.15°$ were used. Coincidence conditions were applied on ^{136}Te ions in BigRIPS and on either the fully stripped or the hydrogenlike ^{136}Te in the ZeroDegree spectrometer (compare Fig. 1). For each of these scattering-angle gated γ-ray spectra the intensity of the 607-keV line was deduced from a fit of the simulated DALI2 response function similar to the ones shown in Fig. 2 for the case of the C target and Fig. 5 for the case of the Au target. In the simulation of the DALI2 response 100% prolate (oblate) nuclear spin alignment was assumed for the Coulomb excitation on the Au target (the nuclear excitation on the C target) [23,24]. A systematic uncertainty of 5%, corresponding to half of the intensity difference obtained for the present detector geometry assuming either 100% prolate (oblate) alignment or no alignment at all, was considered to account for possible attenuation effects from charge state changes and γ decay behind the target. Before the cross section can be calculated for each angular bin, the absolute γ yield has to be corrected for (i) the scattering-angle-dependent losses from the limited acceptance of the ZeroDegree spectrometer, (ii) losses from reactions which take place on any material in the beam line, both targets and beam detectors, between the identifications in BigRIPS and the ZeroDegree spectrometer, and (iii) the charge state fraction. An effective transmission which includes all three contributions can be extracted from the data by comparing the number of ^{136}Te ions which are detected in the ZeroDegree spectrometer (separately for each of the charge states) to the number of ^{136}Te ions identified in BigRIPS as a function of the scattering angle. The resulting transmission curves for the fully stripped component are shown for both the C and Au targets in Fig. 7(b). As illustrated in the inset of Fig. 7(a) for the C target, the angular distributions of the ions identified as ^{136}Te in BigRIPS exhibit tails at large scattering angles which correspond to ions which had been identified as ^{136}Te in BigRIPS but lost neutrons and/or protons before their scattering angle was measured in the PPACs. These tails have been parametrized, extrapolated to smaller scattering angles, and subtracted from the distributions (details are provided in Ref. [38]). Using these corrected angular distributions, new effective transmission curves have been determined as shown in Fig. 7(b). After removal of the tail, higher transmission
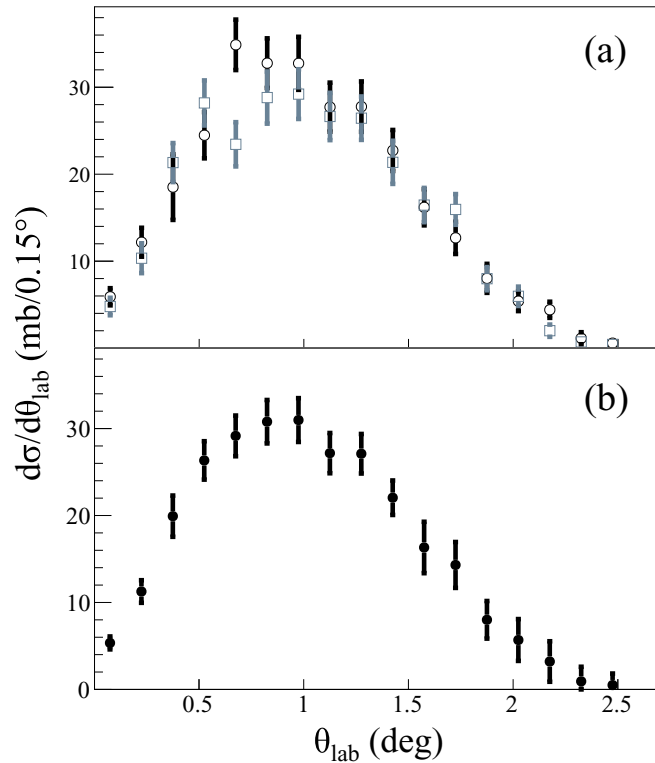
FIG. 8. Experimental cross-section angular distributions measured in coincidence with the 607-keV transition in ^{136}Te on the Au target (a) separately for the ions detected in the fully stripped (open circles) and hydrogenlike (open squares) charge states in the ZeroDegree spectrometer and (b) after averaging both components.

was obtained, in particular for large scattering angles. To acknowledge the uncertainty involved in the subtraction process, an error was assumed for the experimental points at largest scattering angles which covers the full range between the lower limit of the transmission obtained before the subtraction of the tail and the maximum limit corresponding to the assumption of constant transmission over the whole angular range.

Once the effective transmission $T(\text{bin})$ is determined, the cross-section angular distribution is obtained as

$$d\sigma/d\theta_{\text{lab}}(\text{bin}) = \frac{N_\gamma(\text{bin})}{T(\text{bin}) \times N_{\text{ions}} \times d\theta_{\text{lab}}(\text{bin}) \times N_{\text{target}}},$$
(1)

where $N_\gamma(\text{bin})$ is the number of decays of the 2_1^+ state (deduced from the fit to the spectrum for each angular bin), N_{ions} is the number of ^{136}Te ions impinging on the target (number of ions in the BigRIPS gate corrected for the downscaling factor used in the trigger), and N_{target} is the number of target atoms/area. Figure 8(a) shows the resulting cross-section angular distributions $d\sigma/d\theta_{\text{lab}}(\text{bin})$ for the excitation of the 2_1^+ state in ^{136}Te on the Au target, separately for the ions detected in the fully stripped and hydrogenlike charge states, respectively, in the ZeroDegree spectrometer. A good agreement is observed so that finally for each angular bin an average value can be calculated leading to the final cross-

TABLE I. Total cross sections measured in coincidence with γ rays in ^{136}Te on C and Au targets (left) and exclusive inelastic scattering cross sections to individual excited states of ^{136}Te (right). The quoted errors include the uncertainties related to the transmission, the number of γ rays from the fit, the number of detected ions, the target thickness, and the down-scale factor of the trigger. Additional errors of 5% each are added to account for the uncertainties of the DALI2 efficiency calibration and the angular distribution (see text for details).

E_γ (MeV)	σ^C (mb)	σ^{Au} (mb)	E_x (MeV)	I_i^π	σ^C (mb)	σ^{Au} (mb)
0.353	5.1(7)	–	0.607	2_1^+	9.5(32)	219(23)[a]
0.423	10.7(11)	–	1.030	4_1^+	5.6(13)	–
0.607	23(3)	279(22)	1.383	6_1^+	5.1(7)	–
0.810	2.1(3)	–	1.568	(2_2^+)	0.7(5)	–
0.962	2.8(4)	–	2.378	–	2.1(3)	–
3.6	–[b]	21(3)	4.2	–	–	42(4)
4.2	–[b]	21(3)				

[a]Assuming 15(5)% feeding from high-lying 2_x^+ states.
[b]Contaminated by C target excitations.

section angular distribution shown in Fig. 8(b). The total cross section for the excitation of the 2_1^+ state is calculated as sum over all bins, i.e., $\sigma_{\text{tot}} = \sum_{\text{bin}=1}^n d\sigma/d\theta_{\text{lab}}(\text{bin})$. A comparison between Figs. 7(b) and 8(b) shows that the uncertainty in the determination of the transmission in the angular range $\theta_{\text{lab}} > 1.5°$ does not significantly affect the total cross section because the cross-section angular distribution peaks at lower scattering angles.

Note that because of the scattering-angle dependence of the effective transmission and the different shapes of the ion angular distributions and the cross-section angular distributions (see Figs. 7 and 8), a too small cross section value is obtained when it is calculated in an integral way from the total number of γ rays N_γ, and the total transmission $T = N_{\text{ions}}^{\text{ZD}}/N_{\text{ions}}^{\text{BR}}$. In the case of the 2_1^+ state in ^{136}Te excited on the Au target, the difference amounts to 9% for the fully stripped component and 7% for the hydrogenlike ions. In cases in which the statistics is not sufficient to allow for a differential analysis according to Eq. (1), we anticipate that in view of the good agreement between experimental and theoretical cross-section angular distributions to be discussed in Sec. VI, the cross sections can be determined based on the experimental transmission curve and the calculated cross-section angular distribution. All cross-section values measured in coincidence with a discrete γ transition are summarized on the left-hand side of Table I.

To deduce the exclusive excitation cross section to the 2_1^+ state from the cross sections measured in coincidence with the different γ transitions for the C and Au targets, the indirect population of this level from higher-lying excited states has to be considered. For the C target exclusive cross sections have been calculated on the basis of the level scheme presented in Fig. 4. The result is that only less than half of the observed yield of the 607-keV transition, namely $\sigma(2_1^+) = 9.5(32)$ mb, is from the direct excitation of the 2_1^+ state, while the remaining intensity is because of feeding from the higher-lying

states. As mentioned in the last section, two discrete γ rays with energies above 3.5 MeV have been observed following the inelastic excitation of the ^{136}Te ions on the Au target. One of them populates the 2_1^+ state and consequently the cross section of 21(3) mb corresponding to this transition has to be subtracted from the 279(22) mb measured for the 607-keV γ ray (see Table I). In this case the statistics was sufficient to subtract this feeding contribution in a differential way, i.e., separately for each bin of the cross-section angular distribution shown in Fig. 8(b). In addition, the contribution from unobserved feeding from higher-lying 2^+ states has to be taken into account. This feeding fraction was estimated in two different ways. First, this quantity was determined for the experimentally very well-studied stable $N = 84$ isotones ^{142}Ce and ^{144}Nd [25]. In these nuclei, a total of 7 and 12 excited 2^+ states with known lifetimes, respectively, are reported in the energy range from 1.5 to 3.2 MeV. Taking into account measured half-lives and branching ratios, a feeding of 15% and 11% is obtained for the 2_1^+ states in ^{142}Ce and ^{144}Nd, respectively. Alternatively, shell model calculations employing realistic effective interactions (see Sec. VII) have been performed to estimate the feeding from 2^+ states to the 2_1^+ level at 607 keV. In the same energy range quoted above, a total of 16 2^+ states are predicted to exist (see Table 5.6 of Ref. [38]) and from the calculated decay properties, a feeding fraction of 14% is deduced in nice agreement with the experimental numbers for ^{142}Ce and ^{144}Nd. Based on these estimates it is in the following assumed that 85(5)% of the remaining yield measured for the 607-keV γ ray, $\sigma(2_1^+) = 0.85(5) \times 258(22)$ mb $= 219(23)$ mb correspond to the direct excitation of the 2_1^+ state in ^{136}Te.

V. EXTRACTION OF B($E2; 0_1^+ \rightarrow 2_1^+$) FROM THE MEASURED $\sigma(2_1^+)$

In scattering off a high-Z target both electromagnetic and nuclear excitations can occur so that both processes, as well as the interference between them, contribute to the measured inelastic scattering cross section. Therefore, the determination of the B($E2$) value from the measured cross section is not a trivial task. For Coulomb excitation experiments at intermediate or relativistic energies (with typical beam energies between 40 and 180 MeV/u) there are in general four different ways to determine the transition probability for the state of interest, e.g., B($E2; 0^+ \rightarrow 2_1^+$) values, from the measured exclusive inelastic scattering cross section. In the first two, relative measurements are performed. The excitation strength is deduced either by comparison to target excitations with known transition probability (e.g., the 548-keV transition in ^{197}Au; see examples in Ref. [26]) or relative to another nucleus excited under the same experimental conditions [27–29]. In these cases the quality of the obtained result relies mainly on the reliability of the experimental information from literature and the correct evaluation of experimental differences (with respect to transmission, feeding, efficiencies, etc.). In cases in which nuclear contributions cannot be neglected, in addition also possible differences with respect to the nuclear deformation length, δ_{nucl}, have to be considered. Alternatively, two different approaches have been

used in the literature which are based on the measurement of absolute inelastic scattering cross sections. In the analyses of experiments performed at NSCL, using beam energies in the range from 40 to 80 MeV/u, cuts on the scattering angle were applied to limit the analysis to peripheral collisions in which nuclear contributions are assumed to be negligible ("safe" impact parameter criterion touching spheres plus 2 fm); see Refs. [30,31] and overview tables in [32,33]. At the higher beam energies in the order of 150 MeV/u, which are usually employed for experiments at GSI and RIKEN [28,29,34–36], this technique is not valid any longer as will be illustrated below. In these cases, transition probabilities can only be deduced from the measured cross sections when the contributions from both the Coulomb and nuclear interactions to the total cross section are correctly accounted for. This latter approach will be discussed in detail in Sec. VI.

A. The minimum impact parameter (maximum scattering angle) approach

Once the angular resolution of the measurement is determined (see last section and Fig. 7) we can demonstrate why at least in the present case of ^{136}Te measured at a midtarget energy of 139 MeV/u, but probably more in general in this energy domain, the approach to apply a cut on the scattering angle to suppress nuclear contributions to the measured cross section is no longer valid. Using the criterion which is commonly applied in the analysis of NSCL experiments, namely selecting a minimum impact parameter corresponding to touching spheres plus 2 fm, a maximum scattering angle of $\theta_{\max} = 1.2°$ in the laboratory system is calculated for the Au target. Figure 9(a) shows a schematic cross-section angular distribution, $d\sigma/d\theta_{\mathrm{lab}}$, in line with the Alder-Winther formalism [37]. Here it is assumed that all events with angles beyond $\theta_{\max}$ are absorbed, corresponding to a sharp angle cutoff in a simplistic black-disk model. In Figure 9(b), the corresponding cross-section angular distribution is shown for the case of ^{88}Kr excited on a ^{209}Bi target at a midtarget energy of 58.5 MeV/u which was recently discussed in Ref. [31]. In this case, a significantly larger maximum scattering angle of $\theta_{\max} = 3.2°$ is obtained. Now, to compare these theoretical curves with data, they have to be folded with the angular resolution of the experiment which in the present case amounts to $\sigma_{\mathrm{Au}} = 8.8$ mrad as discussed above. This folding is done in three dimensions taking into account independent vectors for the scattering and straggling processes (for more details see Ref. [38]). The comparison between the original and folded curves shown in Fig. 9 legitimates the approach followed by the NSCL group to limit the comparison to angles below a certain limit and only consider the Coulomb part of the interaction (at least in cases in which the nuclear contributions are small; see Sec. VI). A comparison to the Fig. 3 of Ref. [31] indicates that the angular resolution in that experiment was similar to the one assumed here. Depending on the resolution indeed a maximum scattering angle can be chosen, here $\theta = 2.4°$ [31], so that nuclear contributions and absorption effects are negligible [see green dashed line in Fig. 9(b)]. Although proven to be a valid analysis procedure it still has the drawback that for the determination of the transition probability
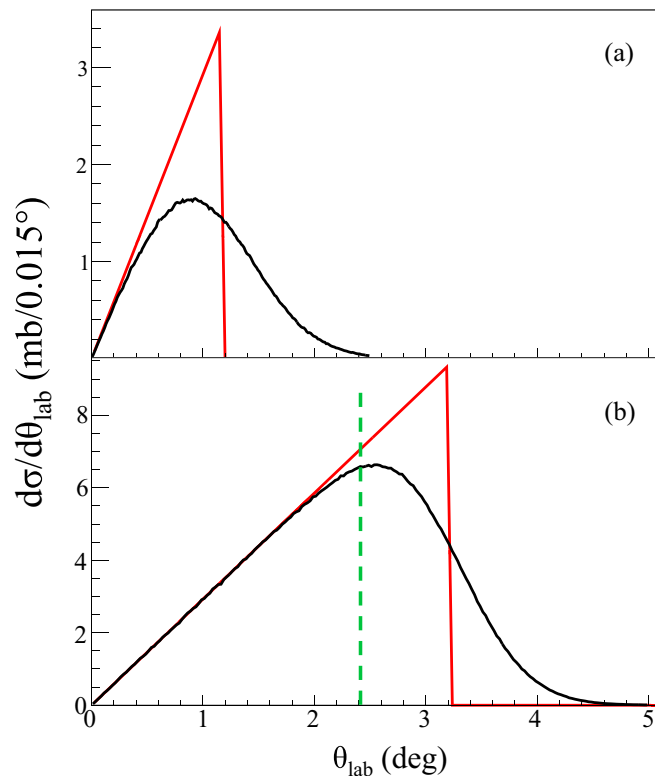
FIG. 9. Illustration of the effect of the limited experimental angular resolution on the measurement of cross-section angular distributions for (a) the reaction ^{136}Te + ^{197}Au at 139 MeV/u discussed in the present work and (b) the reaction ^{88}Kr + ^{209}Bi at 58.5 MeV/u [31]. The red lines correspond to cross-section angular distributions calculated within the relativistic Coulomb excitation model of Ref. [37] and cut at θ_{max}, while the black lines show these theoretical curves after folding with the experimental angular resolution of $\sigma_{Au} = 8.8$ mrad. The dashed green line indicates the more restrictive scattering-angle cut applied in the analysis presented in Ref. [31].

it takes advantage of only part of the statistics gathered in the experiment (roughly 50%). The same comparison for the case of ^{136}Te as shown in Fig. 9(a), on the other hand, clearly demonstrates that this technique cannot be applied in the present case. To conclude, only when the safe scattering angle is large as compared to the angular resolution of the experiment, a cut on the cross-section angular distribution is a valid approach. However, for most of the experiments performed at higher beam energies around 150 MeV/u at GSI and RIKEN this is not the case.

B. Consistent description of both nuclear and electromagnetic excitations with the reaction code FRESCO

As was shown in the last section, in the present case it is not possible to determine a B(E2) value from the measured cross section without considering simultaneously the contributions from both Coulomb and nuclear excitations as well as possible interference effects between them. There are several reaction codes available which allow one to do that, among them ECIS [39], FRESCO [40,41], and DWEIKO [42]. ECIS

and FRESCO are fully quantum-mechanical coupled-channels codes. DWEIKO is also a coupled channels code, designed for inelastic processes, which makes the additional eikonal (i.e., forward-angle, high-energy) approximation to the distorted waves to simplify its solution. The different versions of the ECIS code have widely been used in the past in the analysis of Coulomb excitation experiments [35,36,43–46], in some of these cases considering relativistic kinematics. In particular in the cases in which cross-section angular distributions have been measured with high angular resolution and thus high sensitivity to the interference pattern between the nuclear and Coulomb interactions, ECIS has proven to well describe the experimental data. Unfortunately, ECIS97 shows convergence problems when applied to heavier systems such as the reaction discussed in the present work and therefore had to be discarded. Before using instead the FRESCO code for the determination of the B($E2$; $0_1^+ \rightarrow 2_1^+$) value in ^{136}Te we investigated its capability to correctly describe some of the high-resolution measurements reported in the literature, in particular the cross-section angular distributions measured for excited states in ^{208}Pb populated in collisions with a ^{17}O beam at 84 MeV/u [43,46] as well as the data reported in Ref. [35]. Good agreement was found so that it seems legitimate to employ FRESCO instead of ECIS97 in the present analysis. Unfortunately no experimental information on the cross-section angular distributions for inelastic scattering were found in the literature for heavier systems and at higher beam energies. In the following results will be presented which have been obtained with a modified version of the FRESCO code [47] that takes into account relativistic kinematics. Before closing this section we would like to mention that we were not able to reproduce the cross-section angular distributions measured for the system ^{17}O + ^{208}Pb [43,46] using the DWEIKO code. The analysis of both electric dipole and quadrupole states seems to indicate that, at least in the studied cases, neither the nuclear-Coulomb interferences nor the nuclear absorption are correctly treated.

VI. DETERMINATION OF THE REDUCED TRANSITION PROBABILITY B($E2$; $0_1^+ \rightarrow 2_1^+$)

To deduce a reduced transition probability to the 2_1^+ state in ^{136}Te from the experimental exclusive cross section on the Au target determined as discussed in Sec. IV, both the nuclear and Coulomb contributions have to be considered. In all calculations presented in this section, optical potentials were used which were derived from the microscopic folding model with the complex G-matrix interaction CEG07 and a specific global density (for more details see [48]). For the Coulomb part the standard collective-model form factor was employed. Because in reactions on the C target Coulomb effects are negligible information about the nuclear deformation length can be deduced from the cross sections measured on this light target (compare Table I). The inclusive cross section of $\sigma^C = 23(3)$ mb measured for the 607-keV transition is reproduced with FRESCO using a value for the deformation length of $\delta_{nucl}^{eff} = 1.05(7)$ fm, while the exclusive cross section to the 2_1^+ state, $\sigma^C(2_1^+) = 9.5(32)$ mb, is reproduced with a value of $\delta_{nucl}(2_1^+) = 0.68(10)$ fm. As shown
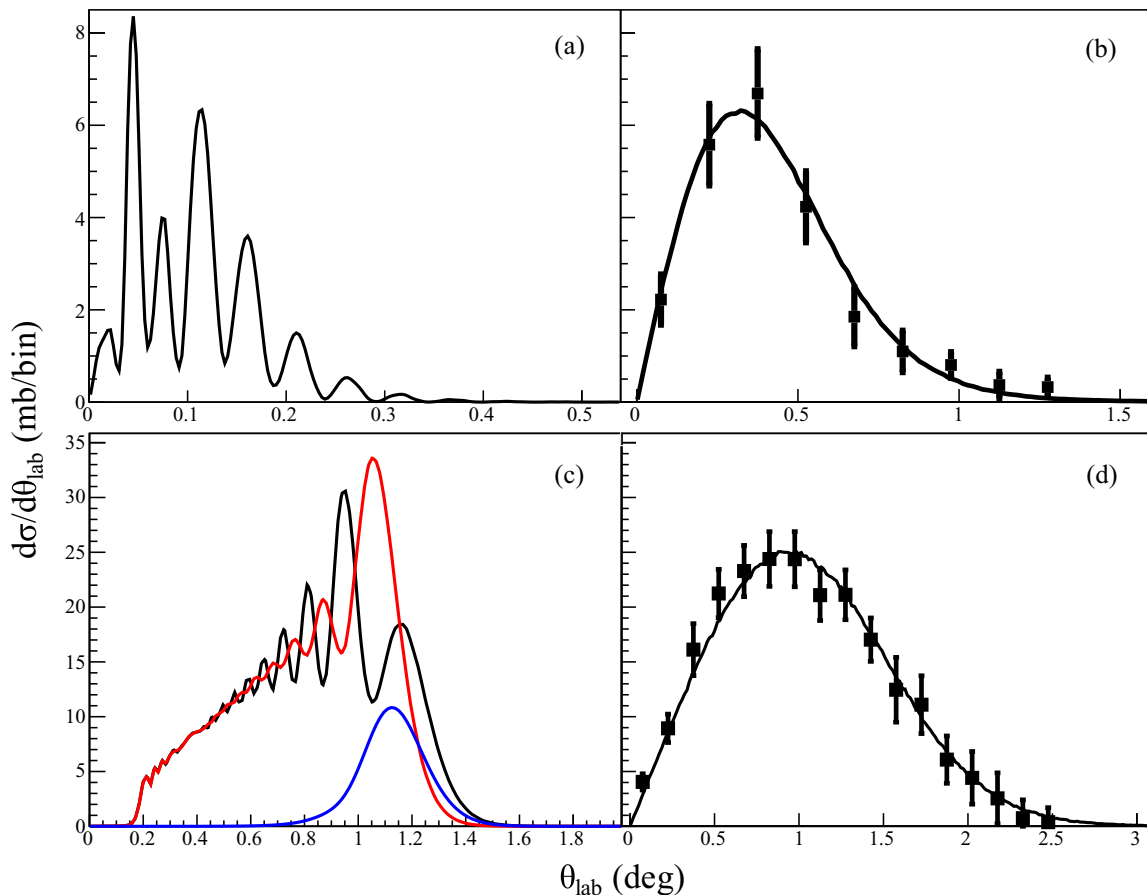
FIG. 10. Theoretical (a) and experimental (b) cross-section angular distributions for the excitation of the 2_1^+ state in ^{136}Te on a C target. In (b) the theoretical curve was folded with the experimental angular resolution following the procedure discussed in the text. Theoretical (c) and experimental (d) cross-section angular distributions for the excitation of the 2_1^+ state in ^{136}Te on a Au target. In (c) in addition to the total differential cross section (black line) the Coulomb (red) and nuclear (blue) contributions are also shown separately. In (d) the theoretical curve was folded with the experimental angular resolution following the procedure discussed in the text. Bins of $0.025°$, $0.15°$, $0.071°$, and $0.15°$ have been used in parts (a)–(d), respectively.

in Fig. 10(a) for the C target the cross section [calculated here for $\delta_{\mathrm{nucl}}^{\mathrm{eff}} = 1.05(7)$ fm] is centered at very small scattering angles. As a consequence, the measured cross-section angular distribution mainly reflects the experimental angular resolution and is thus very sensitive to the correct folding. The theoretical curve after folding is shown in comparison to the experimental data in Fig. 10(b). Nice agreement is observed which validates the folding method. Turning now to the data taken with the Au target, the B($E2; 0_1^+ \rightarrow 2_1^+$) value can be determined taking into account the effective nuclear deformation length, $\delta_{\mathrm{nucl}}^{\mathrm{eff}}$. This approach assumes that the relative population of the different excited states from nuclear interactions is the same for the two targets. Keeping $\delta_{\mathrm{nucl}}^{\mathrm{eff}} = 1.05(7)$ fm fixed, the reduced matrix element $M(E2)$ is varied until the experimental exclusive cross section to the 2_1^+ state, $\sigma^{\mathrm{Au}}(2^+) = 219(23)$ mb, is reproduced. In this way, a value of B($E2; 0_1^+ \rightarrow 2_1^+$) = 0.195(22) e^2b^2 is obtained. Note that the quoted uncertainty is the maximum error from the experimental error of the cross section [$\sigma = 242$ mb are obtained assuming B($E2$)=0.217 e^2b^2 while B($E2$)=0.173 e^2b^2 corresponds to $\sigma = 196$ mb]. The comparison between the experimental cross-section angular distribution and that

calculated with FRESCO and folded with the angular resolution is shown in Fig. 10(d). As in the case of the C target, the theoretical curve reproduces the shape of the experimental distribution somewhat well. Note that the theoretical curves shown in Fig. 10 are not adjusted to the experimental data but the result of calculations, which reproduce the measured total cross section taking into account nuclear contributions. So far all calculations have been performed for beam energies corresponding to the average energy of the ions at the center of the target. The influence of the finite target thickness on the resulting reduced transition probability will be discussed in Sec. VI A.

To illustrate the influence of the nuclear contribution to the total cross section, the calculated total cross-section angular distribution as well as those obtained separately for the Coulomb ($\delta_{\mathrm{nucl}} = 0$ fm) and nuclear [$M(E2) = 0$ eb] parts are shown in Fig. 10(c). The optical potentials affect the shape of the total cross-section angular distribution in two ways. The real part of the potential determines the cross section from nuclear excitations [blue curve in Fig. 10(d)] while the imaginary part is responsible for the absorption, i.e., it defines the right wing of the distribution. The Coulomb and nuclear

interactions interfere in a destructive way, thus leading to a shift of the position of the maximum of the distribution to smaller scattering angles. The destructive interference is also reflected by the nuclear and Coulomb contributions to the total cross section. Coulomb and nuclear cross sections of $\sigma_{\text{Coul}} = 224$ mb and $\sigma_{\text{nucl}} = 44$ mb lead to a total cross section of $\sigma^{\text{tot}} = 219$ mb. Because of the destructive interference, the B($E2$) value is not very sensitive to the nuclear deformation length δ_{nucl}. A smaller value of the latter corresponds to a lower nuclear cross section. In this case, to compensate for the smaller value of σ_{nucl}, the Coulomb cross section would slightly increase to yield the same total cross section σ^{tot}. However, because also the interference changes, these effects are small. As example we quote here the values $\sigma_{\text{Coul}} = 234$ mb and $\sigma_{\text{nucl}} = 19$ mb which are obtained assuming $\delta_{\text{nucl}} = 0.68$ fm, i.e., the deformation length which reproduces the experimental exclusive cross sections to the 2_1^+ on the C target. In this case, the resulting B($E2$) value increases by 4%. Interestingly, assuming $\delta_{\text{nucl}} = 0$ fm, i.e., no nuclear contribution at all, a 2.5% smaller B($E2$) value is deduced from the measured σ^{tot}. Unfortunately, because of the limited angular resolution of the present experiment, the measured cross-section angular distribution is not sensitive to the value of δ_{nucl}.

A further test was made to study the robustness of the result with respect to the optical model potentials used in the calculations. The potentials calculated by Furumoto *et al.* [48] are based on the Sao Paulo parametrizations of the proton and neutron density distributions which are adjusted to stable nuclei. To test the validity of this prescription when applied to neutron-rich nuclei such as ^{136}Te potentials were calculated based on realistic theoretical density distributions which have been calculated with the Hartree-Fock-Bogoliubov approach and the finite range density-dependent Gogny force in the D1S parametrization [49]. Using these potentials instead of the original ones in the analysis, the resulting B($E2$) value changes by less than 2%. Finally, the full analysis was repeated also using optical potentials which were obtained with the t-$\rho\rho$ approximation [50]. In this case a slightly larger deviation of 5% was found for the final B($E2$) value. Thus, to account for the systematic uncertainty related to the choice of the optical potentials a systematic error of 5% was assumed in the present work.

To close this section, we would like to briefly come back to the minimum impact parameter approach discussed in Sec. V A. After having discussed the results of the FRESCO calculations shown in Fig. 10(c) it is clear now that not only the limited experimental angular resolution from straggling and position measurement uncertainties, but also the interference between the Coulomb and nuclear excitations prohibits the use of this approach in the analysis of experiments performed at beam energies around 150 MeV/u. Because of the destructive interference, the total integral cross section up to the maximum scattering angle of $\theta_{\text{max}} = 1.2°$ is about 9% smaller as compared to the integral Coulomb excitation cross section in the same angular range (196 vs 215 mb), so that even in the ideal case of perfect angular resolution a too small B($E2$) value would be obtained when only Coulomb excitation is considered. With respect to the analysis of experiments

performed with beam energies in the range 40–80 MeV, note that although shown to be in many cases a valid approach, using this method implies losing a considerable fraction of the available statistics. At these lower beam energies as compared to the experiment discussed here, the relative contribution of nuclear excitations to the measured cross section is in general smaller (although notable exceptions may exist) and consequently also the interference phenomena are less important. Then the only crucial ingredient for a reliable calculation of the total inelastic scattering cross section is the correct description of the nuclear absorption process for small impact parameters, i.e., large scattering angles. The comparison between the calculated and measured cross-section angular distributions for the 2_1^+ state in ^{136}Te shown in Fig. 10(d), together with those for the studied literature examples mentioned in Sec. V B. and additional experimental cases studied at RIKEN [51], clearly shows that FRESCO calculations using modern optical model potentials provide a realistic description of the measured cross-section angular distributions. It would be very interesting to compare the results obtained following the analysis approach presented here and the one employing a scattering-angle cut for a typical experiment such as the one discussed in Ref. [31].

A. Correction because of the significant energy loss in the thick target

In the thick Au target used in the present experiment (950 mg/cm^2) the ions lose more than 30% of their initial energy during the passage through the target. They slow down from 165 MeV/u to 110 MeV/u. Because the increase of the Coulomb excitation cross section with decreasing beam energy is not linear, the error made when considering in the analysis a fixed energy, namely the energy at the center of the target, in the determination of the B($E2$) value has to be estimated. The cross sections calculated for the average beam energies at the entrance, the center, and the exit of the target are 190, 219, and 267 mb, respectively. To first order the B($E2$) value has to be reduced by 2%, leading to a value of B($E2$; $0_1^+ \rightarrow 2_1^+$) $= 0.191(24)$ e^{2}b^2. An uncertainty of the same order as the effect is assumed. Note that also the shape of the cross-section angular distribution of the inelastically scattered ions changes with the beam energy. However, because of the limited angular resolution of the present experiment these effects are nearly washed out once the theoretical curves are folded with the experimental response.

B. Uncertainty from nonconsideration of relativistic reaction dynamics

As mentioned before in the present work, a modified version of the FRESCO code is used which is taking into account relativistic kinematics. We note that in the present case of the 2_1^+ state in ^{136}Te excited on a Au target at a midtarget energy of 139 MeV/u, a 7% smaller B($E2$) value would be deduced when the standard version of FRESCO [40] would have been employed. For a fully consistent description of the excitation process also dynamical relativistic corrections

TABLE II. Summary of the systematic uncertainties which have been considered in the determination of the final value of B(E2; $0_1^+ \rightarrow 2_1^+$) = 0.191(26) e^2b^2.

	$\sigma^{Au}(2_1^+)$ (mb)	$\Delta\sigma^{Au}(2_1^+)$ (mb)	Error
Inclusive	279	9	Statistical
γ efficiency	279	17	5%
γ ang. distr.	279	22	5%
Feeding	219	23	5%
	B(E2) (e^2b^2)	ΔB(E2) (e^2b^2)	Error
FRESCO	0.195	0.022	$\Delta\sigma^{Au}(2_1^+)$
Potentials	0.195	0.024	5%
Target thickness	0.191	0.024	2%
Rel. dynamics	0.191	0.026	5%

on the nuclear and Coulomb potentials should be taken into account. Based on previous calculations using an eikonal version of the continuum-discretized coupled-channels (CDCC) method [52] these corrections are expected to be somewhat small in the present case. Choosing a conservative approach, we consider an additional systematic uncertainty of 5% in the determination of the final B(E2) value.

C. Summary of systematic uncertainties

The final result of the analysis and the different contributions to its error are summarized in Table II. After taking into account all possible sources of systematic uncertainties related to the different analysis steps, the final relative uncertainty amounts to 14%. It is important to notice that the systematic uncertainties dominate the final error. Because of the high counting statistics of the present experiment, the statistical uncertainty of the cross section measured for the 607-keV transition on the Au target is only 3%. Already at this point the systematic uncertainty of 5% inherent to the determination of the γ-ray intensities from a fit of simulated spectra to the experimental data, i.e., the uncertainty from the efficiency calibration of DALI2, is larger than the statistical error. Because the latter uncertainty as well as the other systematic errors considered in this work, related to the choice of the optical potentials, the relativistic corrections and the finite target thickness, are unavoidable and difficult to reduce, the precision for the reduced transition probability reached in the present work can be considered as a limit of what can be achieved using the technique of Coulomb excitation at relativistic energies at facilities such as RIKEN or GSI/FAIR.

Note that using the equation [42,53],

$$B(E\lambda) = \left(\frac{3}{4\pi}ZeR^{\lambda-1}\right)^2 \delta_{Coul,\lambda}^2, \quad (2)$$

with the radius at 50% of the central nuclear density $R = 1.2 \, A^{1/3}$ fm and the multipolarity $\lambda = 2$, a charge deformation length $\delta_{Coul,\lambda} = 0.57(4)$ fm can be calculated from the B(E2) value. This value is in agreement with the nuclear deformation length $\delta_{nucl} = 0.68(10)$ fm deduced above from the exclusive inelastic scattering cross section to the 2_1^+ state, $\sigma^C(2_1^+)$. Note

that any unobserved feeding, which still may contribute to $\sigma^C(2_1^+)$, would further decrease δ_{nucl}. Equality of the nuclear and charge deformation lengths, $\delta_{nucl} = \delta_{Coul}$, was actually assumed in the analysis of several experiments in the past [45,46]. It is expected to be valid when the neutron and proton distributions are similar and the two nuclei interact only at the surface, which is the case for heavy-ion inelastic scattering being dominated by strong absorption [54].

VII. DISCUSSION

The main experimental result of the present work is the value of the $E2$ transition probability, $B(E2; 0_1^+ \rightarrow 2_1^+) = 0.191(26)$ e^2b^2, to the first excited 2^+ state in ^{136}Te. This value is compared to previous results reported in the literature in Table III and Fig. 11. Our measurement, performed using Coulomb excitation at relativistic energies, agrees with the large value which was recently obtained in Coulomb excitation at safe energies at Oak Ridge [6]. It is, however, in conflict with the low-energy Coulomb excitation measurement of Refs. [1,3] and the preliminary result of the experiment using the fast timing technique reported by Fraile *et al.* [2]. We cannot comment on the discrepancy between the two low-energy Coulex experiments, both performed at HRIBF, which employed a carbon target in one case and a titanium target in the other.

The conflict between the results of the two recent Coulomb excitation experiments on one side and the fast timing measurement on the other, in case the preliminary result of the latter will be confirmed, is very interesting. There are already several other cases in the literature in which discrepancies between the results from Coulomb excitation experiments and those obtained using experimental techniques which allow one to directly extract the lifetime of excited states, e.g., methods based on the Doppler effect, have been observed. One prominent example are the $B(E2; 0_1^+ \rightarrow 2_1^+)$ values of the stable Sn isotopes [58,59]. Therefore, a new direct measurement of the 2_1^+ lifetime is of highest interest.

To compare the experimental $B(E2; 0_1^+ \rightarrow 2_1^+)$ value for ^{136}Te with theory, the results of various theoretical calculations performed in the framework of the nuclear shell model (SM) and the quasiparticle random phase approximation (QRPA) are included in Fig. 11. The theoretical values are taken from Refs. [6] (SM1,SM2), [5] (QRPA), [7] (MCSM),

TABLE III. Comparison of the transition probabilities in ^{136}Te determined in the present work with those reported in the literature.

B(E2; $I_i^\pi \rightarrow I_f^\pi$) ($e^2b^2$)			Reference
$0_1^+ \rightarrow 2_1^+$	$4_1^+ \rightarrow 2_1^+$	$0_1^+ \rightarrow 2_x^+$	
0.122(18)	–	–	Danchev *et al.* [3]
0.122(24)	–	–	Fraile *et al.* [2]
0.181(15)	0.060(9)	<0.02	Allmond *et al.* [6]
0.191(26)	–	<0.019[a]	Present work
0.151(69)	0.061(31)[b]	–	Present work, τ

[a]Assuming a 100% 0.9 MeV decay branch to the 2_1^+ state.
[b]From $\tau_{eff}(4_1^+)$, including feeding from the 6_1^+ state.
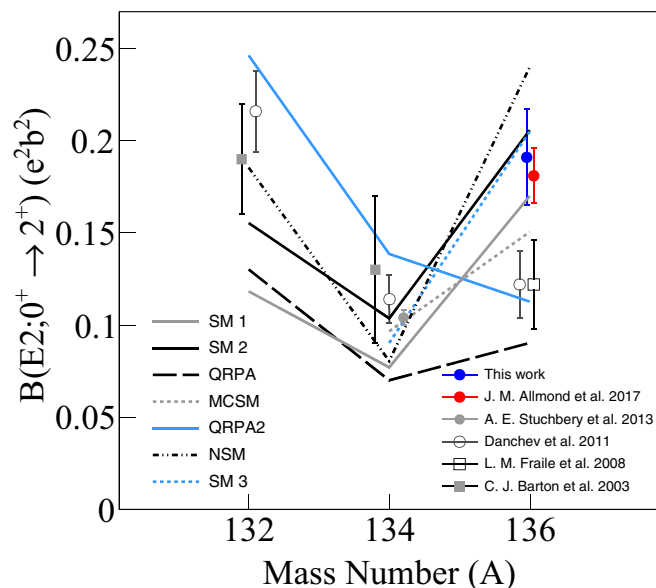
FIG. 11. Comparison of the experimental $B(E2; 0_1^+ \rightarrow 2_1^+)$ value for ^{136}Te determined in the present work to literature values for the ^{132,134,136}Te isotopes [2,3,6,55,56] and different theoretical calculations (SM1,SM2 [6], QRPA [5], MCSM [7], QRPA2 [9], NSM [8], and SM3 [57]).

[9] (QRPA2), [8] (NSM), and [57] (SM3). We note that all the different SM calculations predict large B(E2) values for ^{136}Te close to the one measured in the present work and Ref. [6], while the two QRPA calculations provide smaller E2 strengths closer to the experimental values extracted in Refs. [2,3]. On the other hand, all three SM approaches, which allow one to calculate B(E2) values also for ^{132}Te, namely SM1, SM2, and NSM, predict larger B(E2) values for the $N = 84$ isotope ^{136}Te as compared to the $N = 80$ ^{132}Te, in contrast to the available experimental information. Note, however, that in all three calculations different configuration spaces and effective interactions have been used to describe the nuclei below and above the $N = 82$ shell closure. It will be very interesting to see the results obtained with the most recent SM approaches which consider larger configuration spaces including orbitals above and below the $Z = 50$ and $N = 82$ shell closures and thus allow one to describe isotopic chains across the neutron shell closure on equal footing [60,61].

In Sec. III A. observational lower limits of 10% and 14% relative to the intensity of the 607-keV line have been determined for γ rays with energies of 0.9 MeV and 1.6 MeV, respectively, decaying from a hypothetical mixed-symmetry 2^+ state in ^{136}Te. These limits correspond to lower limits of either 0.019 e^{2}b^2 or 0.027 e^{2}b^2 for the B(E2; $0_1^+ \rightarrow 2_{ms}^+$) value when the exclusive decay via either a 0.9 or a 1.6 MeV γ ray is assumed. To compare the experimental limit to the calculations, in each case the theoretical branching ratio for the

decay branches to the 2_1^+ and 0_1^+ states is taken into account. For the MCSM calculation of Ref. [7] with a branching ratio of 4.6:1, a limit of $B(E2; 0_1^+ \rightarrow 2_{ms}^+) < 0.023$ e^{2}b^2 is obtained which can be compared to the calculated value of $B(E2; 0_1^+ \rightarrow 2_{ms}^+) = 0.03$ e^{2}b^2. The QRPA calculations of Ref. [9] predict a branching ratio of 1.9:1, which leads to an experimental limit of $B(E2; 0_1^+ \rightarrow 2_{ms}^+) < 0.029$ e^{2}b^2 as compared to the theoretical value of $B(E2; 0_1^+ \rightarrow 2_{ms}^+) = 0.074$ e^{2}b^2. Even more illustrative than this comparison between the absolute experimental and theoretical transition strengths is that for the relative strength, i.e., $B(E2; 0_1^+ \rightarrow 2_{ms}^+)/B(E2; 0_1^+ \rightarrow 2_1^+)$. In the case of the MCSM calculation, the theoretical value of 20% compares to the experimental limit <12%, while the QRPA prediction of 66% is much larger as compared to the experimental result <15%. We conclude that currently there is no experimental evidence for an enhanced E2 excitation probability to a 2_{ms}^+ state in ^{136}Te. The experimentally determined upper limits are in agreement with the 2_{ms}^+ predictions of the SM calculations employing realistic effective interactions [4,38].

VIII. CONCLUSIONS

We reported on the in-beam γ-ray spectroscopy of the neutron-rich nucleus ^{136}Te following inelastic scattering on gold and carbon targets at energies around 140 MeV/u performed at the RIBF facility at the RIKEN Nishina Center. A value of $B(E2; 0_1^+ \rightarrow 2_1^+) = 0.191(26)$ e^{2}b^2 was derived from the experimental exclusive inelastic scattering cross section on the Au target, taking into account both the Coulomb and nuclear contributions to the measured cross section. Our B(E2) value is in good agreement with the result of a recent experiment employing low-energy Coulomb excitation [6] but at variance with previously reported values [2,3]. The origin of this striking disagreement among the available experimental information remains an open question, which calls for additional future investigation. Furthermore, an upper limit for the excitation probability for a hypothetical mixed-symmetry 2_{ms}^+ state was established on the basis of the experimental sensitivity. Finally, the high statistics gathered in the present experiment allowed one to perform a model analysis for the determination of B(E2) values from measured differential cross sections after inelastic excitation at relativistic energies which can serve as a guideline for the analysis of future Coulomb excitation experiments performed at beam energies around 150 MeV/u at GSI and RIKEN.

ACKNOWLEDGMENTS

[1] D. C. Radford, C. Baktash, J. R. Beene, B. Fuentes, A. Galindo-Uribarri, C. J. Gross, P. A. Hausladen, T. A. Lewis, P. E.

Mueller, E. Padilla, D. Shapira, D. W. Stracener, C.-H. Yu, C. J. Barton, M. A. Caprio, L. Coraggio, A. Covello, A. Gargano,

D. J. Hartley, and N. V. Zamfir, Phys. Rev. Lett. **88**, 222501 (2002).

[2] L. M. Fraile *et al.*, in *Proceedings of the 23rd International Nuclear Physics Conference*, edited by S. Nagamiya, T. Motobayashi, M. Oka, R. S. Hayano, and T. Nagae (2008), p. 218.

[3] M. Danchev, G. Rainovski, N. Pietralla, A. Gargano, A. Covello, C. Baktash, J. R. Beene, C. R. Bingham, A. Galindo-Uribarri, K. A. Gladnishki, C. J. Gross, V. Y. Ponomarev, D. C. Radford, L. L. Riedinger, M. Scheck, A. E. Stuchbery, J. Wambach, C.-H. Yu, and N. V. Zamfir, Phys. Rev. C **84**, 061306(R) (2011).

[4] A. Covello *et al.*, Prog. Part. Nucl. Phys. **59**, 401 (2007).

[5] J. Terasaki, J. Engel, W. Nazarewicz, and M. Stoitsov, Phys. Rev. C **66**, 054313 (2002).

[6] J. M. Allmond, A. E. Stuchbery, C. Baktash, A. Gargano, A. Galindo-Uribarri, D. C. Radford, C. R. Bingham, B. A. Brown, L. Coraggio, A. Covello, M. Danchev, C. J. Gross, P. A. Hausladen, N. Itaco, K. Lagergren, E. Padilla-Rodal, J. Pavan, M. A. Riley, N. J. Stone, D. W. Stracener, R. L. Varner, and C.-H. Yu, Phys. Rev. Lett. **118**, 092503 (2017).

[7] N. Shimizu, T. Otsuka, T. Mizusaki, and M. Honma, Phys. Rev. C **70**, 054313 (2004); **74**, 059903(E) (2006).

[8] D. Bianco, N. Lo Iudice, F. Andreozzi, A. Porrino, and F. Knapp, Phys. Rev. C **88**, 024303 (2013).

[9] A. P. Severyukhin, N. N. Arsenyev, N. Pietralla, and V. Werner, Phys. Rev. C **90**, 011306(R) (2014).

[10] T. Kubo *et al.*, Prog. Theor. Exp. Phys. **2012**, 03C003 (2012).

[11] N. Fukuda, T. Kubo, T. Ohnishi, H. Inabe, H. Takeda, D. Kameda, and H. Suzuki, Nucl. Instrum. Methods B **317**, 323 (2013).

[12] S. Takeuchi, T. Motobayashi, Y. Togano, M. Matsushita, N. Aoi, K. Demichi, H. Hasegawa, and H. Murakami, Nucl. Instrum. Methods A **763**, 596 (2014).

[13] S. Agostinelli *et al.*, Nucl. Instrum. Methods A **506**, 250 (2003).

[14] K. Butler-Moore *et al.*, J. Phys. G **19**, L121 (1993).

[15] P. Hoff, J. P. Omtvedt, B. Fogelberg, H. Mach, and M. Hellström, Phys. Rev. C **56**, 2865 (1997).

[16] A. Korgul *et al.*, Eur. Phys. J. A **7**, 167 (2000).

[17] V. Vaquero, A. Jungclaus, P. Doornenbal, K. Wimmer, A. Gargano, J. A. Tostevin, S. Chen, E. Nacher, E. Sahin, Y. Shiga, D. Steppenbeck, R. Taniuchi, Z. Y. Xu, T. Ando, H. Baba, F. L. Bello Garrote, S. Franchoo, K. Hadynska-Klek, A. Kusoglu, J. Liu, T. Lokotko, S. Momiyama, T. Motobayashi, S. Nagamine, N. Nakatsuka, M. Niikura, R. Orlandi, T. Saito, H. Sakurai, P. A. Soderstrom, G. M. Tveten, Z. Vajta, and M. Yalcinkaya, Phys. Rev. Lett. **118**, 202502 (2017).

[18] J. R. Terry *et al.*, Phys. Rev. C **77**, 014316 (2008).

[19] A. Lemasson *et al.*, Phys. Rev. C **85**, 041303(R) (2012).

[20] S. Akkoyun *et al.*, Nucl. Instrum. Methods **668**, 26 (2012).

[21] I.-Yang Lee, AIP Conf. Proc. **656**, 343 (2003)

[22] Computer code ATIMA, http://web-docs.gsi.de/weick/atima/.

[23] H. Olliver, T. Glasmacher, and A. E. Stuchbery, Phys. Rev. C **68**, 044312 (2003).

[24] P. Bednarczyk *et al.*, Acta Phys. Pol. B **40**, 853 (2009).

[25] http://www.nndc.bnl.gov.

[26] C. Vaman *et al.*, Phys. Rev. Lett. **99**, 162501 (2007).

[27] V. M. Bader *et al.*, Phys. Rev. C **88**, 051301(R) (2013).

[28] A. Banu *et al.*, Phys. Rev. C **72**, 061305(R) (2005).

[29] G. Guastalla *et al.*, Phys. Rev. Lett. **110**, 172501 (2013).

[30] A. Gade *et al.*, Phys. Rev. C **68**, 014302 (2003).

[31] B. Elman *et al.*, Phys. Rev. C **96**, 044332 (2017).

[32] C. A. Bertulani *et al.*, Phys. Lett. B **650**, 233 (2007).

[33] H. Scheit *et al.*, Phys. Lett. B **659**, 515 (2008).

[34] P. Doornenbal *et al.*, Phys. Rev. C **90**, 061302(R) (2014).

[35] K. Li *et al.*, Phys. Rev. C **92**, 014608 (2015).

[36] P. Doornenbal *et al.*, Phys. Rev. C **93**, 044306 (2016).

[37] A. Winther and K. Alder, Nucl. Phys. A **319**, 518 (1979).

[38] Victor Vaquero Soto, Ph.D thesis, Universidad Autónoma de Madrid, 2018.

[39] J. Raynal, Coupled-channel code ECIS97 (unpublished).

[40] I. J. Thompson, Comput. Phys. Rep. **7**, 3 (1988).

[41] http://fresco.org.uk.

[42] C. A. Bertulani, C. M. Campbell, and T. Glasmacher, Comput. Phys. Commun. **152**, 317 (2003).

[43] J. Barrette *et al.*, Phys. Lett. B **209**, 182 (2008).

[44] P. Roussel-Chomaz *et al.*, Phys. Lett. B **209**, 187 (1988).

[45] T. Motobayashi *et al.*, Phys. Lett. B **346**, 9 (1995).

[46] R. Liguori Neto *et al.*, Nucl. Phys. A **560**, 733 (1993).

[47] A. M. Moro, Phys. Rev. C **92**, 044605 (2015).

[48] T. Furumoto *et al.*, Phys. Rev. C **85**, 044607 (2012).

[49] J. L. Egido (private communication).

[50] M. S. Hussein, R. A. Rego, and C. A. Bertulani, Phys. Rep. **201**, 279 (1992).

[51] T. Arici *et al.* (unpublished).

[52] K. Ogata and C. Bertulani, Prog. Theor. Phys. **121**, 1399 (2009).

[53] G. R. Satchler, Nucl. Phys. A **472**, 215 (1987).

[54] D. L. Hendrie, Phys. Rev. Lett. **31**, 478 (1973).

[55] C. J. Barton *et al.*, Phys. Lett. B **551**, 269 (2003).

[56] A. E. Stuchbery *et al.*, Phys. Rev. C **88**, 051304(R) (2013).

[57] H. Naidja, F. Nowacki, and B. Bounthong, Phys. Rev. C **96**, 034312 (2017).

[58] J. M. Allmond *et al.*, Phys. Rev. C **92**, 041303(R) (2015).

[59] A. Jungclaus *et al.*, Phys. Lett. B **695**, 110 (2011).

[60] T. Togashi *et al.*, Phys. Rev. Lett. **121**, 062501 (2018).

[61] D. Rosiak *et al.*, Phys. Rev. Lett. **121**, 252501 (2018).